

Adherence and electrochemical behavior of calcium titanate coatings onto 304 stainless steel substrate

J. Esguerra-Arce

*TPMR, Escuela de Ingeniería de Materiales, Universidad del Valle,
Calle 13 # 100-00, A.A. 25360, Cali, Colombia,
Tel: +57 2 3244893
e-mail: johanna.esguerra@univalle.edu.co*

Y. Aguilar

*TPMR, Escuela de Ingeniería de Materiales, Universidad del Valle,
Calle 13 # 100-00, A.A. 25360, Cali, Colombia.*

W. Aperador

*Escuela de Ingeniería Mecánica, Escuela Colombiana de Ingeniería Julio Garavito,
AK 45 # 205-59 (Autopista Norte), A.A 14520, Bogotá, Colombia.*

N. Alba de Sánchez

*Grupo de Investigación en Ciencia e Ingeniería de Materiales, Corporación Universidad Autónoma de Occidente,
Calle 25 # 115-85, A.A 2790, Cali, Colombia.*

G. Bolaños Pantoja

*Laboratorio de Física de Bajas Temperaturas, Departamento de Física, Universidad del Cauca,
Calle 5 # 4-70, A.A 996, Popayán, Colombia.*

C. Rincón

*Laboratorio de Física de Bajas Temperaturas, Departamento de Física, Universidad del Cauca,
Calle 5 # 4-70, A.A 996, Popayán, Colombia.*

Received 27 August 2013; accepted 21 March 2014

Calcium titanate has been proposed as a coating for biomedical applications but it has not been reported characterization of adhesion failure mechanisms or electrochemical properties in time. In this work have been studied these properties of a calcium titanate coating growth onto AISI 304 steel deposited by r.f. magnetron sputtering. It was found that the coating has a critical adhesive load of 6.53 ± 0.14 N. With respect to its electrochemical properties potentiodynamic polarization curves show that the calcium titanate coating provides protection to AISI 304 steel. However, EIS indicates that even though metal dissolution occur through the pores in the coating, this leads to the precipitation of salts that block pores; this precipitates layer acts like an additional barrier to the metal dissolution in the system.

Keywords: Biomaterials; calcium titanate coating; magnetron sputtering; scratch test; corrosion.

PACS: 68.60.Bs; 68.35.Np; 82.45.Bb

1. Introduction

A hip prosthesis is an artificial device that replaces or complements a hip joint lost through trauma, disease or congenital conditions. Although bioceramics are used in many types of medical procedures and they are more biocompatible than metals, they are fragile and less resilient, so that hip prosthesis stems are made of three types of metal: titanium alloys, cobalt-chromium-molybdenum (Co-Cr-Mo) alloys and austenitic stainless steel (316L or 316N). Titanium and its alloys have been successfully used due to their high mechanical strength, biocompatibility, and durability and corrosion resistance in physiological environments [1]. Co-Cr-Mo alloys that meet ASTM F75 standard [2] are also widely used in orthopedic implants manufacture. Especially these alloys present excellent biocompatibility and a good combination of corrosion resistance with good mechanical and tribologi-

cal properties [3]. Stainless steels are also widely used in hip stems mainly due to its high corrosion resistance and good mechanical properties.

Due to the high cost of titanium and its alloys and their poor tribological properties, stainless steels are still used in hip prosthesis and remain under investigation for biomedical purposes [4-7], which is why this article proposes to study AISI 304 stainless steel as a substrate to be used as prosthesis stem, as this is used as a biomaterial and has been widely used in implants such as brackets and screws. This steel also meet ASTM F138 y ASTM F139 [8,9] standards for steels used in biomedical applications and it is cheaper than AISI 316L which would represent a reduction in hip prosthesis cost.

Hip prosthesis stems may be cemented or uncemented. In cemented prosthesis cement adheres the stem to the bone, while in uncemented one bonding is due to the design, a porous surface or by a bioactive coating facilitating bone at-

TABLE I. Chemical composition of Hank's solution, concentration [g/L].

NaCl	KCl	MgSO ₄ ·7H ₂ O	CaCl ₂ ·H ₂ O	Na ₂ HPO ₄	KH ₂ PO ₄	NaHCO ₃	Glucosa
8.0	0.4	0.2	0.185	0.046	0.06	0.35	1.0

tachment. The only commercially used coating for this application is hydroxyapatite in titanium femoral stems [10-12]. Since hydroxyapatite is osteoconductive [1] a direct bone apposition occurs that provide coupling of the implant to the surrounding bone. These coated prostheses have presented a big clinical success, as they increase the rate of osseointegration regarding uncemented prosthesis [13,11]. However, with time this coating detaches exposing the base metal [12], which can lead to loosening of the prosthesis.

Calcium titanate has been proposed like bio-coating for this kind of applications since it was found as an interface layer in hydroxyapatite coatings onto titanium alloys [14,15]. Some authors have obtained calcium titanate layers by various methods on titanium and titanium alloys, such as sol-gel [16], magnetron sputtering [17], ion-beam assisted deposition [18], pulsed laser deposition [19], hydrothermal-electrochemical method [20], thick alkalized calcium oxidation [21] and hydrothermal treatment [22] for biomedical applications.

An implant should possess appropriate adherence and electrochemical in order to serve for a long period of time without rejection. Coatings for orthopedic implant applications are subject to external forces and it is important and necessary to know their adhesion and failure modes [23]; and it is important to understand the electrochemical behavior of coatings for implants because of the possible release of ions from the substrate toward medium [24], which can result in adverse biological reactions which in turn can lead to mechanical failure of the device [25].

Therefore, this work aims to evaluate calcium titanate coating growth onto AISI 304 stainless steel by r.f. magnetron sputtering, evaluating adherence by scratch test and electrochemical properties by electrochemical impedance spectroscopy (EIS) and polarization curves.

2. Materials and methods

The CaTiO₃ cathode used for sputtering technique were prepared by the following sintering method: CaTiO₃ powder with a purification of 99.9% from Super Conductor Materials, Inc., was compacted into a 5.08 cm diameter disk by cold press (150 MPa), and then sintered at 1200°C for 4 hours.

The coatings deposition was carried out via magnetron sputtering during 4 hours at 500°C. The crystal structure of the films was determined by using glancing incident X-ray diffraction (GIXRD) at 2° incidence angle with a RIGAKU (Dmax2100) diffractometer using Co K α radiation ($\lambda = 1.78899 \text{ \AA}$, 30 kV and 16 mA). The chemical composition of deposited films was performed by impedance dis-

persive X-ray spectroscopy (EDX) in the scanning electron microscope (JEOL JSM-649 OLV SEM). The thickness of the films was measured by Scanning Electron Microscope (JEOL JSM-649 OLV) and the grain size and the roughness was obtained using an atomic force microscopy (AFM) from Asylum Research MFP-3D $\text{\textcircled{R}}$ using a cantilever silicon tip in non-contact mode and calculated by a Scanning Probe Image Processor (SPIP $\text{\textcircled{R}}$)

Adherence of the layer was studied onto three samples using a Scratch Test Microtest MTR2 system (ASTM C1624-05 [26]), with a scratch length of 1 mm and a raising load of 10 N. To identify the different adherence failures Scanning Electron Microscope (JEOL JSM-649 OLV) and Optical Microscope Olympus BHM were used.

For electrochemical evaluation (three uncoated steel samples and three coated samples were used) a GAMRY Model PCI 4 was used, performing electrochemical impedance spectroscopy (EIS) (ASTM G3-89 [27]) and electrochemical polarization (ASTM G59-97 [28]) techniques at 37°C. The test samples served as working electrode with an exposed area of 1 cm² with a reference electrode Ag/AgCl and a counter electrode of platinum in Hank's solution as an electrolyte (Table I). An analysis of the worn surfaces was performed using a Scanning Electron Microscope (JEOL JSM-649 OLV).

3. Results and discussion

3.1. Chemical composition, morphology and phase composition of the coatings

The EDS spectrum of elemental composition of the coating surface revealed a Ca-Ti ratio of 0.98, and the SEM observation showed a thickness of 750 nm.

The XRD pattern of sintered CaTiO₃ indicates that it exhibits orthorhombic Pbnm crystal structure [29]. This is in accordance with Roushoun Ali *et al* [30], who indicate that calcium titanate exhibit this symmetry in the temperature range of 23 - 1225°C.

The grazing incident XRD pattern of CaTiO₃ layer is shown in Fig. 1. This indicates that the coating exhibits polycrystalline structure with a (022) preferential orientation corresponding to Pbnm orthorhombic CaTiO₃ phase at 33.293° [29,31], cubic Pm-3m calcium titanate [32], TiO₂ anatase phase [33] and CaO [34].

The grain size and roughness measured by AFM (Fig. 2) were 43.8 \pm 0.1 nm and 4 nm, respectively. Although grain size of calcium titanate coatings has not been reported in previous works, it is known that in context of osteoblast and protein adsorption as the grain size as the roughness are relevant,

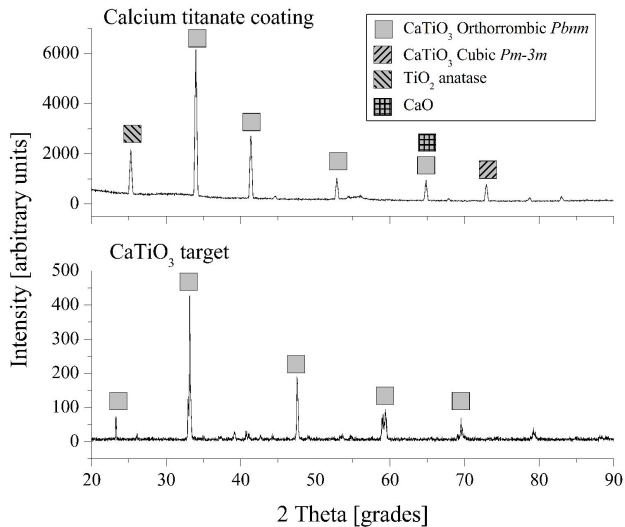


FIGURE 1. GI-XRD patterns of the calcium titanate coating.

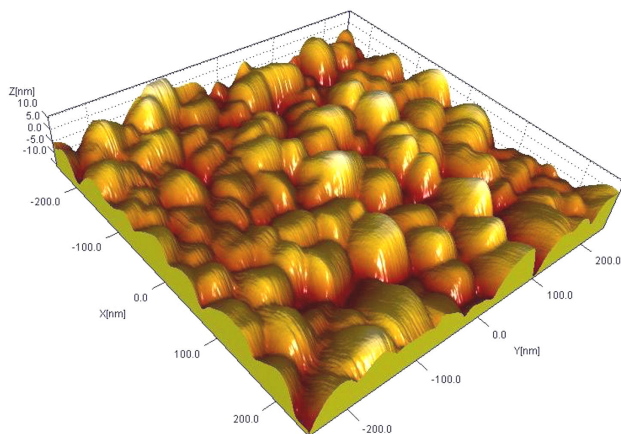


FIGURE 2. AFM image of calcium titanate coating grown on AISI 304 steel with a Ti buffer layer.

since both occur at nano- and micro-scale [35,36], so that the values of grain size and roughness found here can be beneficial in adhesion and proliferation of bone cells. This grain size is consistent with that reported by Nelea *et al* [37], who obtained HA coatings by magnetron sputtering on Ti-5Al-2.5Fe having grains within average size of 20-30 nm.

3.2. Adherence

After drawing the diamond stylus across the flat surfaces, the analysis was conducted by observing micrographs of the wear track and correlating the values of displacement in stylus drag coefficient vs. normal load curves to determine the loads at which each failure mode occurs.

Comparing with Fig. 3 in [38] Fig. 3 shows that failure modes present are angular cracks, semi-circular transverse cracks, which can be seen in detail in c-1); chipping coating, which can be observed in detail in c-1) and a-1); coating breakthrough, as shown in a), b) and c); and the total substrate exposure as observed in the right of a), b) and c). In

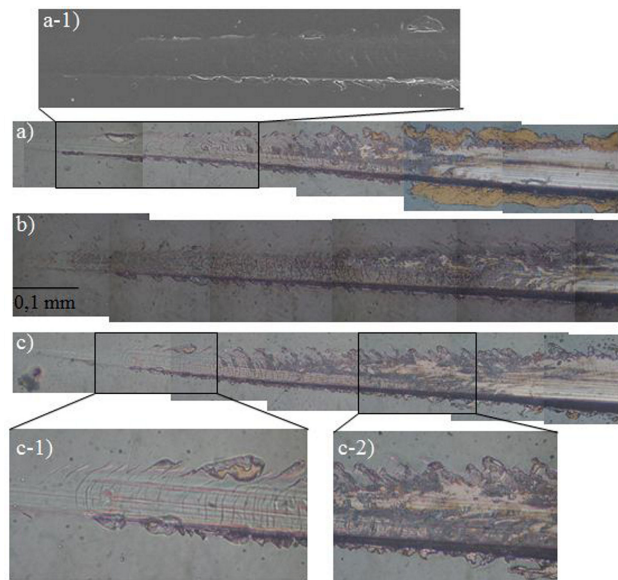


FIGURE 3. a), b), c) Optical images of scratch test track for three calcium titanate coated AISI 304, samples 1, 2 and 3, from top to bottom; c-1) and c-2) zoom from track in sample 3; a-1) SEM image from a portion of track in sample 1.

none on the three samples are presented parallel cracks nor spalling. Observing a) it might seem that there is a coating chipping before the first angular crack appears in sample 3, but it is confirmed that it is not, evaluating the scratch test crack by scanning electron microscopy, as is shown in a-1). Due to this coatings failure development three critical values of load L_{C1} , L_{C2} y L_{C3} was established. In this case L_{C1} , which is related to coating cohesive failure, is the load at which initiate the first angular crack, whose generation can be explained because the need of the coating to release the stress imposed by the indenter; L_{C2} is the load at which coating chipping initiate; and L_{C3} is the load at which appears the first exposure substrate, therefore it is related to adhesive failure of the coating. Figure 4 shows stylus drag coefficient vs. normal load curves for sample 1, where the load values were determined by the distances obtained from optical microscopy images. In these curves is confirmed that, as already mentioned by other authors [39], some failure modes occur without a noticeable change in the curve, so it is evident the need to corroborate and correlate these curves with micrographs of the scratch test crack.

It can be concluded that the calcium titanate coatings on steel AISI 304 obtained by magnetron sputtering with the parameters indicated above show a critical cohesive load $L_{C1} = 1.20 \pm 0.32$ N, and a critical adhesive load $L_{C3} = 6.53 \pm 0.14$ N. This values are higher than those reported by J.A. Toque *et al* [39], which report values lower than 1.2 N in a micro-scratch test on hydroxyapatite coatings with thickness between 1.3 and 2.0 μm on AISI 316L steel obtained by r.f. magnetron sputtering.

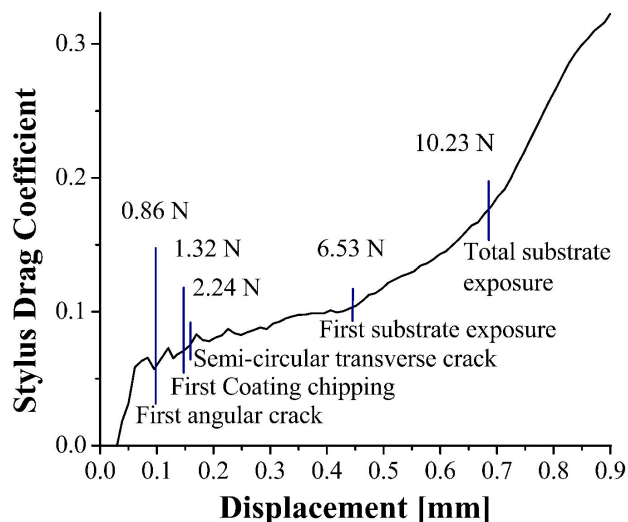


FIGURE 4. FStylus drag coefficient vs. normal load curves for sample 1.

3.3. Electrochemical properties

3.3.1. Polarization measurements

It can be appreciated in Fig. 5 that the curve representing the layer is above than the corresponding to AISI 304 indicating that the corrosion potential of this is more positive and hence there is less prone to corrosion in aggressive medium, equally it is noted that this curve is shifted to the left which allows inferring that the corrosion current density is lower in layer respect to the substrate. It means that the calcium titanate coating obtained by magnetron sputtering provides protection to AISI 304 steel to effectively reduce its sensitivity to corrosion in Hank's solution which is consistent with the findings of Tang Hui [40] in AZ31 alloy coated with calcium titanate. Obtaining anodic and cathodic slopes polarization

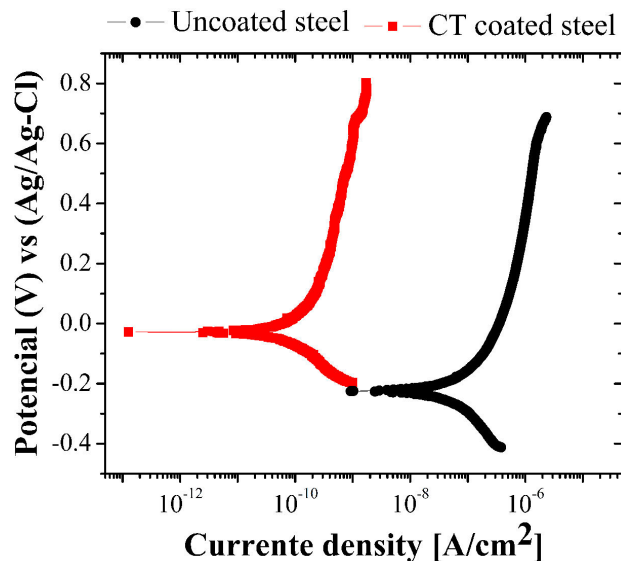


FIGURE 5. Potentiodynamic polarization curves of uncoated steel AISI 304 steel and calcium titanate coatings grown on AISI 304 steel.

resistance values were calculated, with values of 9.31×10^5 ohm-cm² for uncoated steel and 6.00×10^8 ohm-cm² for coated steel.

3.3.2. Electrochemical impedance spectroscopy measurements

Figure 6 shows the Nyquist plots for uncoated steel and calcium titanate coated steel in Hank's solution. The measurements were performed after 1, 24, 360 and 720 hours of immersion in the solution, in order to evaluate the corrosion behavior of the coating at different times of immersion in Hank's solution. In part a) it can be seen the typical impedance spectra for an uncoated steel [41]. In coated steel

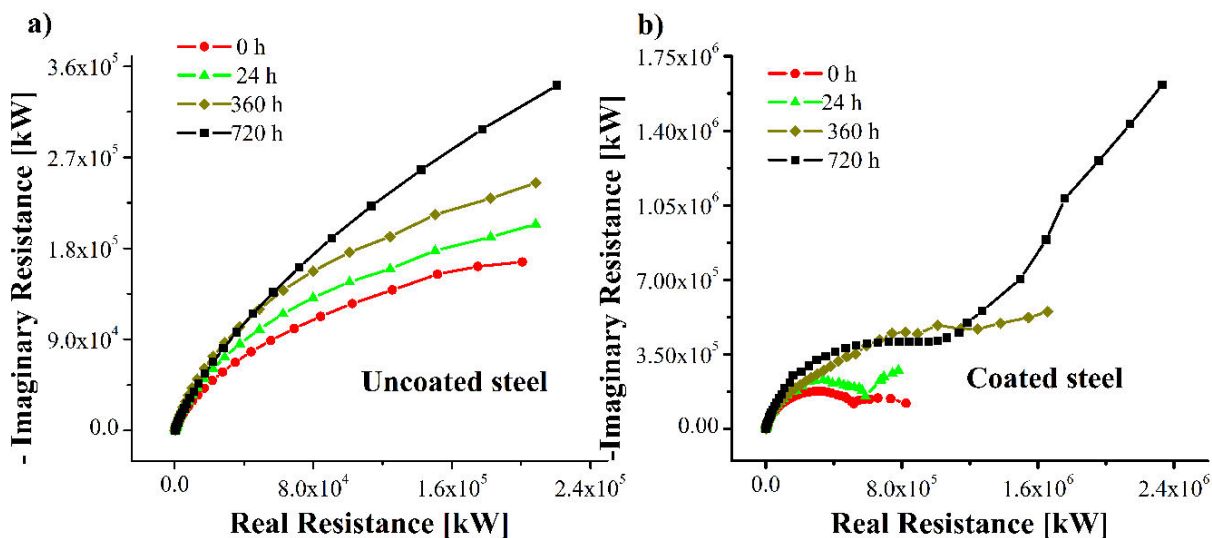


FIGURE 6. Nyquist impedance diagrams of a) uncoated AISI 304 steel and b) calcium titanate coatings grown on AISI 304 steel.

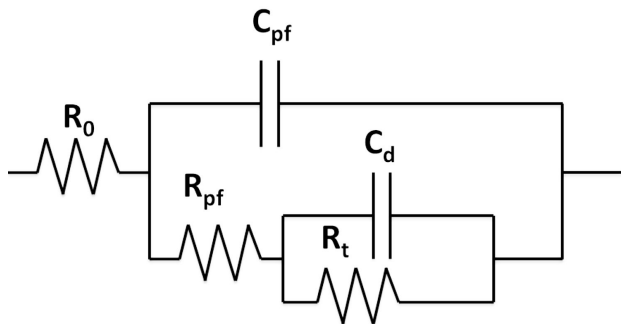


FIGURE 7. Electrical equivalent circuit used to fit the impedance data of calcium titanate coated AISI 304 steel.

it can be seen that the impedance spectra exhibit two time constants in all exposure times, that is, it may be divided into two regions of different frequencies: a time constant in the high frequency arising the uncompensated ohmic resistance due to the electrolyte solution and the impedance characteristics resulting from the penetration of the electrolyte through a porous film, and a time constant in the low frequency of the processes taking place at the interface substrate/electrolyte [41]. This behavior is typical of a coated

metal with a porous film exposed to an electrolytic environment and can be described by the equivalent circuit shown in Fig. 7, where R_0 is the resistance of the electrolyte, C_{pf} is the capacitance of the intact film (or areas of the film where rapid dissolution does not occur), R_{pf} is the pores film resistance due to the electrolyte penetration, C_d is the capacitance of the double layer and R_t is the resistance to metal charge transfer [41].

Figure 8 shows the information obtained from Bode plots. Part a) shows the bode plots of impedance and phase angle for uncoated steel and calcium titanate coated steel at 360 hours. For uncoated steel at low frequencies the phase angle does not reach 0, it approaches a value between -30 and -40, which suggest diffusive processes on solid phase [42] which is no longer observed in calcium titanate coated steel. It is also observed an increase in impedance of the coated steel with respect to the uncoated steel, indicating a corrosion resistance increment of the steel when is coating with calcium titanate [43]. It can be seen in part b) that phase angle diminishes in the steel when is coated with calcium titanate, which points to a less capacitive behavior [41].

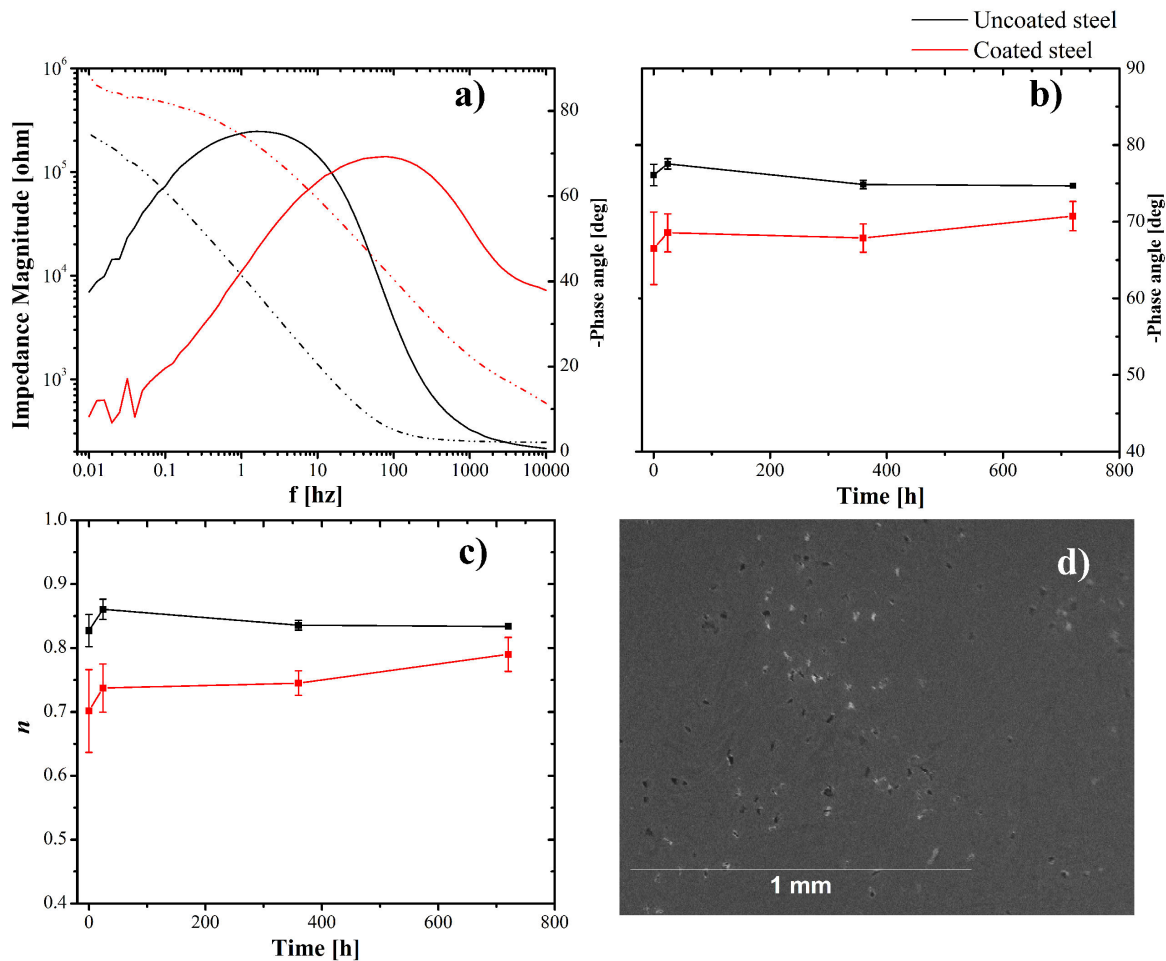


FIGURE 8. Bode information: a) Impedance bode (---) and phase angle bode (—) diagrams at 360 hours, b) phase angle vs time, c) n vs time for uncoated AISI 304 steel and calcium titanate coatings grown on AISI 304 steel and, d) SEM micrograph for calcium titanate coated AISI 304 steel after 720 h in EIS test.

The n behavior in function of time is shown in Fig. 8c), where n is the phenomenological coefficient obtained from the slope of the linear part of the impedance Bode diagram [44]. A value of $n = 1$ represents a purely capacitive behavior, therefore, as in part b) it indicates that the calcium titanate coated steel exhibits a less capacitive behavior than uncoated steel. However, with increasing time it can be seen that the phase angle and the n value of bare steel and coated steel tend to be equal, which could mean that the coated steel capacitance tends to be the uncoated steel capacitance with time. This indicates that even though metal dissolution occurs through the pores in the coating, precipitation of salts that block pores occur. This precipitate layer act like an additional barrier to the metal dissolution in the system [45], which is evidenced by the increase in the resistance values measured with time in Nyquist diagrams in Fig. 6b). Finally, there is evidence of presence of pores in the coating in Fig. 6d), probably the pores that are blocked with precipitated salts.

4. Conclusions

Failure modes of calcium titanate coating on AISI 304 steel measured by scratch test are, in order of appearance, angular

cracks, semi-circular transverse cracks, spalling of the coating and substrate exposure. The coating presents a critical cohesive load L_{C1} of 1.20 ± 0.32 N and a critical adhesive load L_{C3} of 6.53 ± 0.14 N.

Using potentiodynamic polarization curves was found that calcium titanate coating obtained by magnetron sputtering provides good protection to AISI 304 steel because, compared to uncoated steel, coated steel corrosion potential moves toward more positive values and the corrosion current density moves toward more negative values.

EIS test allowed finding that coated steel is less capacitive than uncoated steel. However, even metal dissolution occurs through the pores in the coating, this leads to the precipitation of salts that block pores. This precipitates layer acts like an additional barrier to the metal dissolution in the system.

Acknowledgments

Johanna Esguerra Arce thanks to “Departamento administrativo de ciencia, tecnología e innovación -COLCIENCIAS” for the doctoral fellowship. The authors thanks to professor Liliana del Socorro Tirado Mejía from Laboratorio de Optoelectrónica, Universidad del Quindío, Colombia for help in bulk calcium titanate DRX test.

1. J. D. Bronzino, *The Biomedical Engineering Handbook: Biomedical Engineering Fundamentals, Medical Devices and Systems/Tissue Engineering and Artificial Organs* (Tercera edición, Taylor and Francis Group, 2006).
2. ASTM F75 - 07. *Standard Specification for Cobalt-28 Chromium-6 Molybdenum Alloy Castings and Casting Alloy for Surgical Implants* (UNS R30075), (West Conshohocken, PA, American Society for Testing and Materials, 2007).
3. T.M Wright and S. B. Goodman, *Rosemont*, (IL: American Academy of Orthopaedic Surgeons. 1996). 41.
4. M. Lundin *et al.*, *J. Colloid Interface Sci.* **366** (2012) 155.
5. F.L. Nie, S.G. Wang, Y.B. Wang, S.C. Wei, and Y.F. Zheng, *Dental materials* **27** (2011) 677.
6. F. Barragán, R. Guardián, C. Menchaca, I. Rosales, and J. Uruchurtu, *Int. J. Electrochem. Sci.* **5** (2010) 1799.
7. Y. C. T Tang, S. Katsuma, S. Fujimoto, and S. Hiromoto, *Acta Biomaterialia* **2** (2006) 709.
8. ASTM F138 - 08: *Standard Specification for Wrought 18Chromium-14Nickel-2.5Molybdenum Stainless Steel Bar and Wire for Surgical Implants* (UNS S31673), (West Conshohocken, PA, American Society for Testing and Materials, 2008).
9. ASTM F139 - 08: *Standard Specification for Wrought 18Chromium-14Nickel-2.5Molybdenum Stainless Steel Sheet and Strip for Surgical Implants* (UNS S31673), (West Conshohocken, PA, American Society for Testing and Materials, 2008).
10. J. Faig-Martí and F.J. Gil-Mur, *Rev. esp. cir. ortop. traumatol* **52** (2008) 113.
11. M. Rökkum, *J. Arthroplasty.* **14** (1999) 689.
12. A. E. Porter, P. Taak, L. W. Hobbs, M. J. Coathup, G. W. Blunn, and M. Spector, *Biomaterials* **25** (2004) 5199.
13. M. J. Coathup, G. W. Blunn, N. Flynn, C. Williams, and N. P. Thomas, *J. Bone Joint Surg. [Br]*, **82-B** (2000) 118.
14. C. Ergun, R. Doremus, and W. Lanford, *J. Biomed. Materi. Res. A* **65** (2003) 336.
15. T. Kokubo, H.M. Kim, and M. Kawashita, *Biomaterials* **24** (2003) 2161.
16. S. Holliday and A. Stanishevsky, *Surf. Coat. Technol.* **188** (2004) 741.
17. K. Asami, N. Ohtsu, K. Saito, and T. Hanawa, *Surf. Coat. Technol.* **200** (2005) 1005.
18. N. Ohtsu, K. Saito, K. Asami, and T. Hanawa, *Surf. Coat. Technol.* **200** (2006) 5455.
19. N. Ohtsu, A. Ito, K. Saito, and T. Hanawa, *Surf. Coat. Technol.* **201** (2007) 7686.
20. J.P. Wiff, V.M. Fuenzalida, J.L. Arias, and M.S. Fernandez, *Mater. Lett.* **61** (2007) 2739.
21. N. Ohtsu, C. Abe, T. Ashino, S. Semboshi, and K. Wagatsuma, *Surf. Coat. Technol.* **202** (2008) 5110.
22. J.W. Park *et al.*, *Appl. Surf. Sci.* **257** (2011) 7856.
23. B. Ben-Nissan, B. A. Latella, and A. Bendavid, *Comprehensive Biomaterials* **3** (2011) 63.

24. A. Sargeant, and T. Goswami, *Mater. Design* **28** (2007) 155.
25. N. J. Hallab, S. Anderson, T. Stafford, T. Glant, and J. J. Jacobs, *J. Orthopaed. Res.* **23** (2005) 384.
26. ASTM C1624 - 05 (Reapproved 2010): Standard Test Method for Adhesion Strength and Mechanical Failure Modes of Ceramic Coatings by Quantitative Single Point Scratch Testing, West Conshohocken, PA, (American Society for Testing and Materials, 2005).
27. ASTM G3 - 89 (Reapproved 2010): Standard Practice for Conventions Applicable to Electrochemical Measurements in Corrosion Testing, West Conshohocken, (PA, American Society for Testing and Materials, 2010).
28. ASTM G59 - 97 (Reapproved 2009): Standard Test Method for Conducting Potentiodynamic Polarization Resistance Measurements, West Conshohocken, (PA, American Society for Testing and Materials, 2009).
29. A.V. Arakcheeva, D.Y. Pusharovskii, V.M. Gekimyants, V.A. Popov, and G.U. Lubman, *Kristallografiya* **42** (1997) 54.
30. R. Ali and M. Yashim, *J. Solid State Chem.* **178** (2005) 2867.
31. X. Liu, R.C. Liebermann, *Phys. Chem. Miner.* **20** (1993) 171.
32. H. Fuess, *Fachbereich Materialwissenschaft, Technische Hochschule Darmstadt, Germany* (Private Communication, 1991)
33. V.I. Khitrova, M.F. Bundule, and Z.G. Pinsker, *Kristallografiya* **22** (1977) 1253.
34. W. Z. Gerlach, *Phys.* **9** (1922) 184.
35. R.D.K. Misra, C. Nune, T.C. Pesacreta, M.C. Somani, and L.P. Karjalainen, *Acta Biomater.* **9** (2013) 6245.
36. K. Suzuki, K. Aoki, and K. Ohya, *Bone* **21** (1997) 507.
37. V. Nelea, C. Morosanu, M. Iliescu, and I.N. Mihailescu, *Surf. Coat. Technol.* **173** (2003) 315.
38. K. Holmberg, A. Laukkanen, H. Ronkainen, K. Wallin, and S. Varjus, *Wear* **254** (2003) 278.
39. J.A. Toque, M. K. Herliansyah, M. Hamdi, A. Ide-Ektessabi, and I. Sopyan, *J. Mech. Behav. Biomed.* **3** (2010) 324.
40. H. Tang and F. Wang, *Mater. Lett.* **93** (2013) 427.
41. G. W. Walter, *Corros. Sci.* **26** (1986) 681.
42. M. Metikosš-Huković, E. Tkalčec, A. Kwokal, and J. Piljac, *Surf. Coat. Tech.* **165** (2003) 40.
43. V.A. Alves, *Corros. Sci.* **51** (2009) 2473.
44. B. A. Boukamp, *Solid State Ionics* **18-19** (1986) 136.
45. R. M. Souto, M. M. Laz, and R. L. Reis, *Biomaterials* **24** (2003) 4213.